JOURNAL OF SPACECRAFT AND ROCKETS
Vol. 47, No. 3, May–June 2010

Control Effects of Baffle on Combustion Instability in a LOX/GH_2 Rocket Engine

Songjiang Feng,* Wansheng Nie,† Bo He,‡ and Fengchen Zhuang†
Academy of Equipment Command & Technology, 101416 Beijing, People's Republic of China

DOI: 10.2514/1.46240

The combustion instability encountered unexpectedly in hot-firing tests of the YF-960 liquid oxygen/gaseous hydrogen (LOX/GH_2) rocket engine was numerically researched. Here, the emphasis was on evaluating the control effects of two kinds of baffle configurations on combustion instability. The integrated physical model and numerical method were presented to solve the turbulent, three-dimensional, two-phase, and full-size LOX/GH_2 rocket combustion process. The dominant oscillation frequency characteristics that appeared in the hot-firing tests were reproduced and confirmed first, which validated the computational fluid dynamics code to a certain extent. The baffle effects were investigated by the developed mass flow flux perturbing model. Results show that the control effect of the hub-and-six-blade baffle on the one-order tangential-mode oscillation frequency of 5800 Hz is better than that of the hub-and-three-blade baffle. Although the two kinds of baffles have similar effects on the radial-mode instability, the control effect is better for damping the 5800 Hz oscillation than the 2900 Hz oscillation. This research has provided direct design data for engineers, and it is valuable in further understanding the baffle-eliminating mechanisms.

Nomenclature

A	=	injection cross-sectional area, m^2
C_D	=	droplet drag coefficient
C_{pert}	=	perturbing coefficient
D_m	=	initial mean diameter of LOX droplets, μm
K	=	perturbation constant
$\bar{m}$	=	steady inlet mass flux, kg/s
$\dot{m}$	=	mass flow rate, kg/s
O/F	=	oxidant-fuel mass flow ratio
S	=	source term
T_g	=	injection temperature of H_2, K
u	=	initial velocity of LOX droplets, m/s
$\mathbf{V}$	=	velocity vector, m/s
W_{CH}	=	combustion reaction rate, $\text{kg} \cdot \text{mol}/(\text{m}^3 \cdot \text{s})$
Γ_ϕ	=	exchange coefficient
θ	=	spray angle of LOX droplets, rad
μ_g	=	molecular weight of H_2, kg/mol
ρ	=	density, kg/m^3
ϕ	=	dependent variables
ω_m	=	angular frequency, rad/s

Subscripts

g	=	gas phase
p	=	liquid phase

I. Introduction

THE problem of combustion instability in LOX/GH_2 rocket engines has become increasingly serious as the thrust performance is improved and the operational range is enlarged. It is important and valuable to research and solve the combustion instability in LOX/GH_2 rocket engines. Baffles are often used to control combustion instability. However, combustion flowfields and acoustic characteristics in the chamber become more complex because of the baffle installation, as do the engineering technology, weight, and cooling requirements. And the baffle design projects developed previously are not suitable for all engines. Hence, the investigation of the control effects and mechanisms of different kinds of baffle configurations on LOX/GH_2 rocket engines is important and useful in deciding which kind of baffle projects should be adopted. A number of experiments have been conducted to study the control effects and damping mechanisms of baffles in the LOX/GH_2 rocket engine since the 1960s [1–4]. For example, the control effects of 17 injector face baffle configurations on the combustion instability in a 20,000 lb thrust hydrogen–oxygen rocket were evaluated with a hydrogen temperature at which screech was encountered [1].

However, the experiments are usually costly and time consuming. As the capability of computational fluid dynamics (CFD) increases greatly, the combustion processes of a liquid rocket engine can also be studied by CFD simulation. The linear and nonlinear characteristics of acoustic waves in baffled combustion chambers were studied numerically through perturbation-expansion techniques [5,6]. The results indicated that several specific effects of baffles could be regarded as the eliminating mechanisms, including the longitudinalization of transverse waves inside baffle compartments, the restriction of velocity fluctuations near the injector face, and the decreasing the oscillation frequency. Important features of the energy cascade among acoustic modes were also elucidated when using limit cycle theory, including energy balance in limit cycles and energy transfer by nonlinear gas dynamics. A numerical methodology was developed to predict the acoustic behaviors in the KSR-III engine [7]. The stability margins were evaluated for the optimized design with a hub-and-six-blade baffle. The acoustic fine-tuning of gas–liquid scheme injectors was studied numerically for the acoustic stability of a liquid rocket engine [8]. Additionally, a numerical model was developed to predict the high-frequency combustion instability in liquid rocket engines [9,10]. Variations of the baffle length and the droplet size were found to have an important effect on combustion stability. Controls of combustion instability through various passive devices, including baffles, Helmholtz resonators, and quarter-waves, were computed and compared [11]. The supercritical injector flows and flame dynamics of LOX/GH_2 rocket engines have been researched as an emphasis and have inspired almost worldwide interest recently [12–15].

The combustion processes in oxygen/hydrogen rocket engines have been studied numerically by our team in the last decade [16,17]. Recently, the high-frequency combustion instability that appeared unexpectedly in the hot tests of a hydrogen–oxygen rocket engine

Received 5 July 2009; revision received 13 January 2010; accepted for publication 13 February 2010.

*Ph.D., Department of Space Equipment; hnfengsj@163.com. Student Member AIAA (Corresponding Author).
†Professor, Department of Space Equipment.
‡Ph.D., Department of Space Equipment.

(YF-960) has attracted our interest greatly. As a basic foundation for this work, the influence laws of operational conditions on the combustion instability of the engine have been researched [18]. The hydrogen-injection temperature limits at which oscillations were encountered have been obtained at different oxidant-fuel mass flow ratios and chamber pressures. The variation laws and the frequency characteristics have been also analyzed. In the present work, the control effects of different kinds of baffle configurations were predicted by numerical simulation of the entire combustion chamber. The convergence studies indicated that grid independence was achieved. The comparison with the hot-test data indicated excellent quantitative prediction of the combustion characteristics. The oscillation frequency characteristics were reproduced and confirmed. The control effects of two kinds of baffled injector configurations (a hub-and-three-blade baffle and a hub-and-six-blade baffle) on combustion instability were evaluated to provide the design data for future engines. The control mechanisms of baffle installation were further explored.

II. Physical Model

A comprehensive steady-state combustion model and its submodels are presented in detail in [19]. Considering the tradeoff between the model's complexity and the necessary computer resources, the researchers adopted a liquid spray distribution model, the discrete droplet model, the droplet high-pressure vaporization model, the k–ε two-equation turbulent model, the eddy-break-up model, and the one-step global chemical reaction model.

A. Governing Equations

The injector of the LOX/GH_2 rocket engine consists of concentric tube elements. A concentric tube is a central oxidizer tube surrounded by a concentric fuel annulus, named the shear coaxial injector. Oxygen is mostly in the liquid state. After passing the regeneration cooling channels of the chamber wall, the liquid hydrogen is heated and turned into a gaseous phase when entering the injector. Thus, the turbulent combustion of LOX/GH_2 in the chamber was studied numerically.

The computational formulation for the combusting spray field involves a coupled Eulerian–Lagrangian procedure. The gas-phase equations are solved by an Eulerian, finite volume method, whereas the spray field is computed by a Lagrangian, particle-tracking procedure. The gas and liquid phases are mutually coupled through a series of source terms. Therefore, the combustion processes in the chamber are described by Navier–Stokes equations with different source terms that represent evaporation, chemical reaction, and other two-phase transfer processes. The three-dimensional governing equations were expressed in the general form as follows [20]:

$$\frac{\partial \rho_k \phi_k}{\partial t} + \frac{\partial}{\partial x_j}(r_k \rho_k u_j^k \phi_k) = \frac{\partial}{\partial x_j}\left(r_k \Gamma_\phi \frac{\partial \phi_k}{\partial x_j}\right) + \frac{\partial}{\partial x_j}\left(\phi_k D_{\phi,k} \frac{\partial r_k}{\partial x_j}\right) + S_{\phi,k} + S_{m,\phi,k} + S_{c,\phi,k} \tag{1}$$

where the subscripts $k = 1, 2$ denote the gas and liquid phases, respectively. The momentum equation of the LOX droplets is as follows:

$$\frac{\mathrm{d}\mathbf{V}_P}{\mathrm{d}t} = \frac{3}{8}\frac{\rho_g}{\rho_p}\frac{C_D}{r_p}(\mathbf{V} - \mathbf{V}_P)|\mathbf{V} - \mathbf{V}_P| \tag{2}$$

Equations of the vaporization rate, droplet radius, and droplet temperature are listed in [19]. The gas–liquid equilibrium of LOX/GH_2 and its physical characteristics at high-pressure conditions were considered. The thermodynamic properties and the transport properties were calculated by the Soave–Redlich–Kwong equations of state and the corresponding state principles, respectively [21].

B. Spray Model

The spray model is used to provide the initial conditions and boundary conditions in the numerical simulation, which have important influences on the numerical results. The initial distributions of size, velocity, and position of LOX droplets should be obtained by the spray model. Because the spray process is very complicated, the spray size distribution usually can be calculated by the Rosin–Rammler model. However, the initial mean size used in this model is evaluated mostly by cold tests or experiences. In this paper, the spray model [2] for the LOX/GH_2 axial shear injector was employed to compute the initial mean diameter of the LOX droplets. Then, the spray distributions were achieved by the Rosin–Rammler model [19].

The initial mean diameter of the LOX droplets was expressed as follows [2]:

$$D_m = k\left(\frac{O}{F}\right)\sqrt{\frac{\mu_g A_g}{R\rho_p T_g} P_C} \tag{3}$$

Assuming the uniformity of the velocity distribution, the initial velocity and spray angle were written as follows based on the mass conservation:

$$u = \frac{\dot{m}}{\rho_p A_p} \tag{4}$$

$$\frac{\theta}{2} = \tan^{-1}\left[\frac{4\pi}{C_A}\sqrt{\frac{\rho_g}{\rho_p}}\frac{\sqrt{3}}{6}\right] \tag{5}$$

Based on the given physical and configurable parameter, the initial spray parameters of the shear coaxial injector were obtained from the LOX spray model, including initial size, velocity, and position. Based on the spray experimental data, the value of D_m evaluated by Eq. (3) was suitable when k was 0.01 for the injector and operational conditions here.

C. Turbulence Model

The turbulent flow has an important effect on the mixing and combusting processes in a rocket engine. For the unsteady two-phase turbulent combustion flowfield, both the direct numerical simulation and the large eddy simulation are time consuming. To model turbulence effects practically, the standard k–ε model was adopted. This model has been widely and successfully used in numerically simulating the combustion processes in hydrogen–oxygen rocket engines [13]. It can save the computational load under the condition of ensuring the necessary precision of the three-dimensional simulation. Previous exercises in [20] indicated that the turbulence model was quite robust to be used in performing the numerical simulations for the combustion instability study presented in this paper. Wall function treatment [22] was employed at zones near wall. In addition, the terms for the spray interaction were also considered. For the collision between the LOX droplets and wall, the model originated by Tabakoff and Hamed [23] was employed. The breakup process of the LOX jet and the collision process of the LOX droplets were predicted by the wave model [24] and the O'Rourke model [25], respectively.

D. Chemical Reaction Model

In the present study, three chemical species (H_2, O_2, and H_2O) were assumed, and the H_2/O_2 global chemical reaction mechanism was employed. The Arrhenius mechanism R_{Arr} and turbulent fluctuation mechanism R_{EBU} were used as the control mechanisms of the combustion reaction. The combustion reaction rate was written as follows:

$$W_{\mathrm{CH}} = \min(|R_{\mathrm{EBU}}|, |R_{\mathrm{Arr}}|) \tag{6}$$

E. Combustion Instability Model

It is important to numerically simulate the initial disturbance using the combustion instability model. The amplitude, phase, and space distribution of the disturbance are the necessary parameters. There are three initial disturbance models: the random disturbance model, the pulse pressure model, and the oscillation mode model. The details are presented in [16]. In [9], the pressure perturbing model was developed as follows:

$$p(0, y, t) = \bar{p}(0, y, 0)[1 + C_{\text{pert}} \cos(\omega_m t)] \tag{7}$$

While computing the oscillation frequency in the hot-firing test of the LOX/GH_2 rocket engine described herein, the pressure perturbing model was employed. Similarly, the combustion process also can be influenced by the disturbance of the inlet mass flow flux. One of the active control mechanisms [26] was to adopt the antiresonance mode. In this way, the partial propellant inlet mass flux is adjusted in real time to cause the heat release rate fluctuation to be out phase with the pressure oscillation when instability takes place. In this work, the mass flow flux perturbing model was developed and employed through perturbing the steady-state mass flow flux field at one or some injector inlets with one frequency mode for several cycles:

$$m(x, y, z, t) = \bar{m}(x, y, z, t)[1 + K \sin(2\pi f(t - t_c))] \tag{8}$$

The initial perturbed density and the temperature can be calculated by the isentropic relations. Evidently, when K is greater than 1.0, the negative flux will appear. Although avoiding the negative flux is attempted in practice, this phenomenon really exists in a short period of time near some injectors exit zone when combustion instability takes place. If K is less than 1.0, the oscillation will be too small to analyze when the perturbation is added to only one or a few injector inlets. This has been proven by our practical tests. Therefore, the value of K was assigned to be greater than 1.0 for exciting larger combustion vibration in this paper.

III. Computational Methodology

The numerical solutions were obtained using the research CFD code developed at the Propulsion Theory and Technique Laboratory (PTTL). The finite volume method was used to discretize the governing Navier–Stokes equations in space. The particle source in cell method [27] was adopted to compute the two-phase turbulent combustion flowfield. The gas flowfield was computed to obtain the flowfield parameters, such as temperature, pressure, velocity, and so on. Here the solution was generally convergent. Then, based on the gas field, the tracks of LOX droplets and parameters of droplets along the tracks were computed. The source term of droplets was also computed and applied to every gas-phase equation. And the gas flowfield was obtained again until the solution was convergent. The program was repeated from the second step until the solution was convergent. The parameters of droplets were obtained last. The pressure implicit of splitting operator (PISO) algorithm was extended and used to compute the gas flowfield. Diffusion terms were approximated by a central difference scheme, and convection terms were dispersed by a second-order accuracy upwind scheme. It is confirmed that the PISO algorithm can be used to simulate the combustion instability [16].

IV. Computational Grids and Boundary Conditions

A. Computational Grids

To study the control effect of different baffle configurations on the combustion instability using a three-dimensional full-size numerical simulation, three kinds of chambers with the same geometrical dimensions and different baffle configurations were introduced. They were the chamber without baffle, the chamber with one-hub-and-three-blade baffle, and the chamber with one-hub-and-six-blade baffle, respectively. The axial computational domain ranged from the injector faceplate inlet to the nozzle exit. The aforementioned shear coaxial injector was employed. Figures 1a and 1b show the one-hub-and-three-blade baffle and the one-hub-and-six-blade baffle, respectively. The grids of the partial zone of the injector face and wall are shown in Figs. 2a and 2b, respectively. The triangle nonstructural grids were adopted for the injector face, the injector inlets, and the chamber exit. The quadrangular structural grids were adopted for the wall, including the baffle wall. In the chamber, the triangle-prism grids were generated. Grids were clustered near the

a) One-hub-and-three-blade baffle

b) One-hub-and-six-blade baffle

Fig. 1 Baffle configurations.

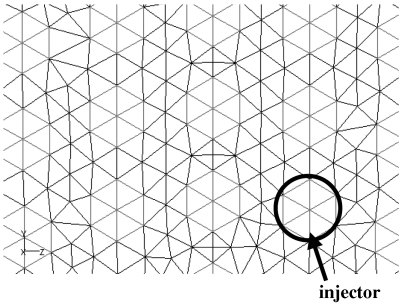

a) Injector face

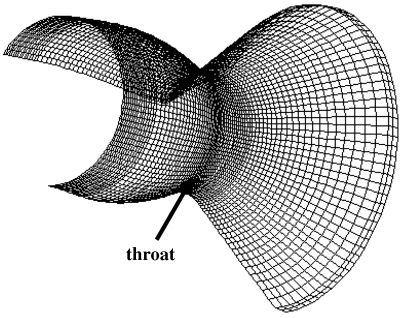

b) Wall

Fig. 2 Partial zone grids of the chamber.

injector faceplate, baffle wall, and nozzle throat to enhance the precision.

Grid independence is an extremely important element of any CFD study. To save the cost of running, the grid-independence tests were tentatively conducted aiming at a shear coaxial single element LOX/GH_2 injector employed by the chamber. Four different numbers of grids for the single injector were used to study the grid independence: 20,600 (grid 1), 156,885 (grid 2), 335,940 (grid 3), and 476,540 (grid 4). This was the basis for verifying the chamber grid independence and developing an adequate grid size for the total chamber. To further verify the chamber grid independence, three levels of grid were generated for the same chamber without baffle based on the single injector grid-independence tests discussed in Sec. V.A. The first level contained 507,528 grid cells (coarse grid), the second level 694,512 (medium grid, based on grid 3), and the third level 1,041,768 (fine grid).

B. Boundary Conditions

For H_2, the inlet mass flow rate $\dot{m}_H$ and temperature T_H were given.

For O_2, the LOX spray particle phase inlet parameters that included temperature T_O and mass flow rate $\dot{m}_O$ were given. The initial mean diameter D_m, the initial velocity u, and the spray angle θ of the LOX droplets were calculated using the spray model, and the droplet distribution was calculated according to the Rosin–Rammler function.

At the exit of nozzle, a second-order extrapolation was applied. The chamber and the faceplate walls were assumed to be no-slip and adiabatic walls.

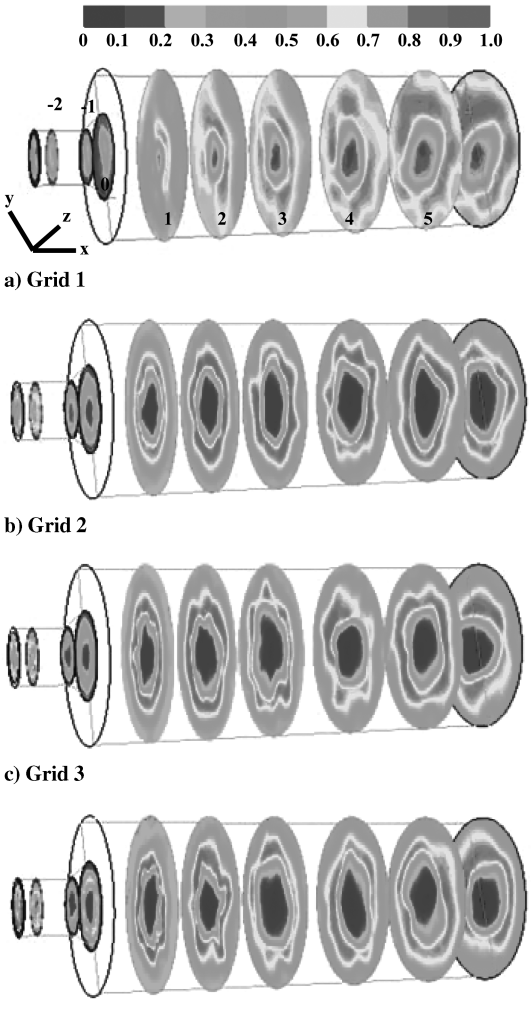

a) Grid 1

b) Grid 2

c) Grid 3

d) Grid 4

Fig. 3 H_2O mass fraction contours at each inspected surface of different grids for the single injector grid independence.

V. Simulation Results and Discussion of Combustion Instability

A. Grid-Independence Tests and CFD Code Validations

Grid dependency on the flow solution was investigated in the present study. Figure 3 shows the result of the grid-independence tests for the single injector by comparing the H_2O mass fraction contours at each inspected surface. It is clear that there is a significant influence of the grid level on the accuracy of the solution. Grid 1 attains a combustion flowfield solution quite different from those computed with the other three grids. The structures of combustion flowfield obtained by grids 2, 3, and 4 are reasonable and accordant on the whole. Though running with grid 4 or an even finer grid would be desirable, the cost for running those finer grids requires an unbearable run time. Because of the limit of the amount of calculations and time, it is impossible to use a much bigger grid than the one used in this study. Therefore, the medium grid size (grid 3) was adopted for the single injector chamber. The grid required for the three-dimensional full-size cylindrical chamber based on grid 3 was evaluated.

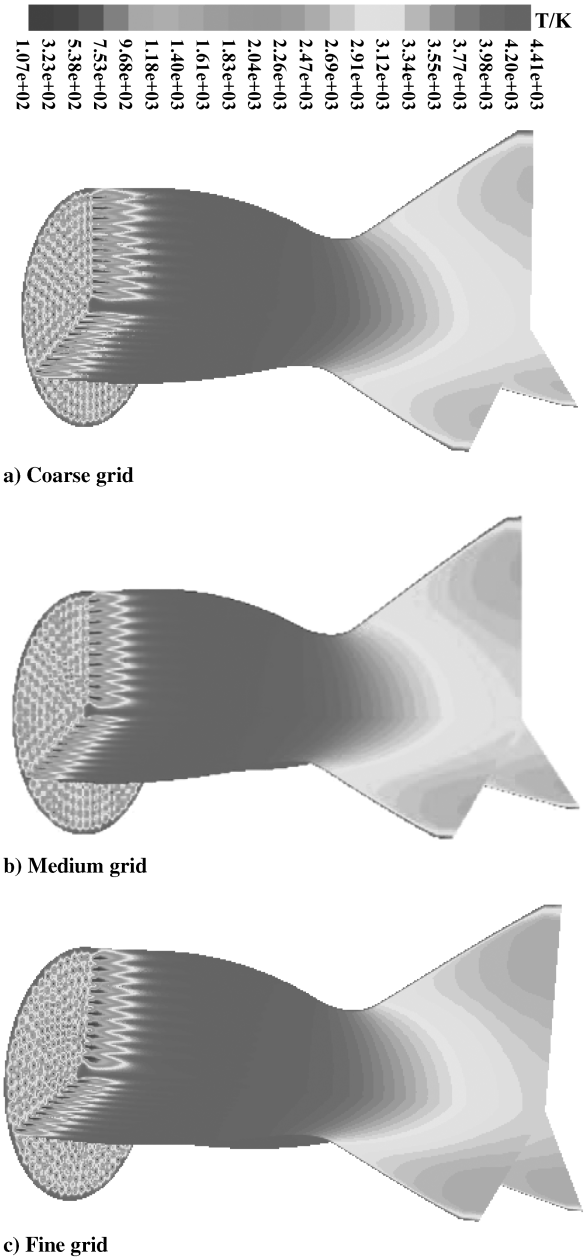

a) Coarse grid

b) Medium grid

c) Fine grid

Fig. 4 Temperature fields of different grids for the no-baffled chamber grid independence.

A dependency analysis was further conducted for the three-dimensional full-size chamber computations. Figure 4 shows the result of the grid-independence tests for the chamber without baffle by comparing the temperature fields. The results of the medium and fine grids, which are similar, are a little more accurate than those of the coarse grid. It shows that the chamber grid generated based on grid 3 is proper. No further computation with an increased number of grid points has been performed, due to the very large CPU time required for the three-dimensional computations. However, the specified grids are believed to be fine enough to give grid-independent solutions.

Moreover, it is very important to conduct the CFD code validation to assess the required fidelity and accuracy. The combustion instability computational methodology and models mentioned earlier have been an important part of the integrated program for liquid rocket engine design conducted by PTTL for many years. The evaporation and combustion of a nondilute spray droplet group under high pressure were studied [28]. The PISO algorithm can be used to simulate the combustion instability successfully, which has been confirmed [16]. The combustion stability maps of the YF-860 LH_2/LOX rocket engine and NAL LOX/methane rocket engine were numerically simulated and the results were in good agreement with the testing data. Additionally, the code was successfully applied to simulate the combustion processes in the LOX/LH_2 rocket engine [20].

In the present study, the CFD code validations were mainly conducted by comparing the numerical results to the hot-test data. The steady-state combustion flowfield in a chamber without a baffle was to provide validation data sets for CFD predictions. The numerical combustion efficiency was about 0.972, computed from the numerical pressure, temperature, combustion gas flow rate, and the nozzle configuration size. It was in reasonable agreement with the hot-test combustion efficiency of 0.98. Additionally, it was shown that the frequency of the combustion instability was in good agreement with the hot-test frequency, which is discussed in Sec. V.C. In a word, the CFD code in this paper has the confidence to numerically simulate the combustion characteristics in the LOX/GH_2 rocket engine.

B. Steady-State Combustion Flowfields

The converged steady-state combustion flowfields under hot-test operational conditions were computed first for the initial conditions of the unsteady computation. It was the foundation for investigating the control effect of baffles on combustion instability through perturbing the steady-state inlet fields. Figures 5a and 5b show the instantaneous contours of temperature field in the chamber with a hub-and-three-blade baffle (baffle 1) and the chamber with a hub-and-six-blade baffle (baffle 2), respectively. The temperature field in the chamber without a baffle is shown in Fig. 4b. Additionally, because there is only hydrogen flow through the baffled injector at the border area, which is different from the other baffled injectors, the temperature at the baffled injector border area of the latter two kinds of chambers is lower than that of the chamber without a baffle.

C. Reproducing of the Pressure Oscillation Encountered in Hot Tests

Based on the steady combustion flowfield in the chamber without a baffle, the pressure perturbing model at all injectors, where C_{pert} was 0.1 and ω_m was 36,424, was used to excite the combustion oscillation. Figure 6 shows the pressure oscillation at the check point (0.01, 0.0705, 0.1354 mm). Figure 6a shows that, although the perturbing coefficient is small, the pressure oscillation is very violent. Additionally, the main frequencies are shown in Fig. 6b.

The result of the numerical simulation of the combustion oscillation basically reproduced and confirmed the oscillation phenomenon in the hot tests. The unwanted pressure oscillation was detected at each pressure check point in the hot tests. And the oscillation frequencies were presented as multiple frequencies of about 2900, 5800, and 8700 Hz, shown in Fig. 7. The maximum peak-to-peak dynamic pressure of the hot tests reached about 24%. Evidently, 2900 Hz is the most noticeable fundamental frequency.

The reason for the difference between the numerical and experimental frequencies may be that the simulated flame temperature is a little higher according to the assumption of the simplified H_2/O_2 reaction mechanism. Flame temperature is intimately associated with heat release, and heat release is intimately associated with combustion instability. In fact, higher temperatures in the chamber obtained

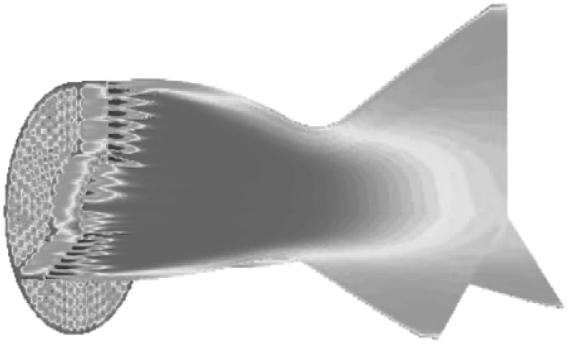

a) Baffle 1

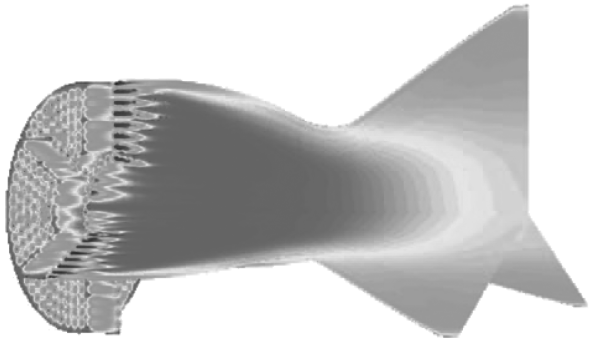

b) Baffle 2

Fig. 5 Contours of the temperature field in two kinds of baffled chambers.

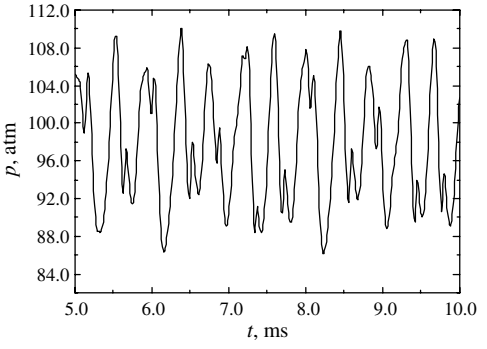

a) Pressure oscillation

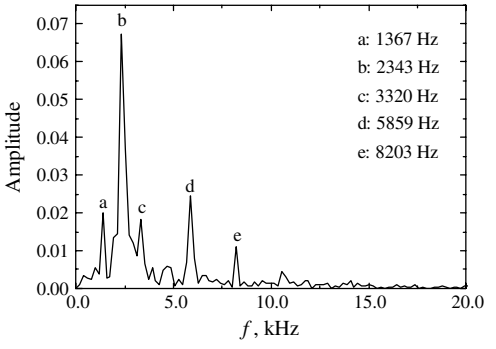

b) Frequency characteristic of the oscillation

Fig. 6 Pressure oscillation characteristics at the check point in the no-baffle chamber.

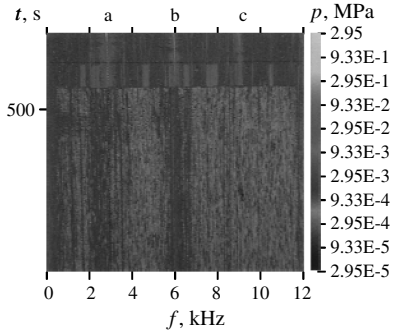

Fig. 7 Pressure oscillation characteristic of the hot test.

by simulation resulted in higher sound speeds. As a result, the calculated chamber frequencies were in general agreement with those observed in the test, especially for 5800 Hz. Together, the simulated main frequencies of 2343 and 3320 Hz may describe the tested frequency characteristic of 2900 Hz. That the simulated frequencies were in general agreement with the hot-test frequency also provided the CFD code validation again.

The influence laws of operational conditions on the combustion instability of the engine have been previously researched [18]. Here, based on the oscillation frequency characteristics that appeared in the hot tests, the control effects of the two kinds of baffle configurations mentioned earlier on combustion instability were especially evaluated. In addition, the control mechanisms of baffle installation were further explored.

D. Control Effects on Tangential-Mode Instability

The mass flow flux perturbing model was used to analyze the control effects of baffles on the combustion instability. The vibration of the injected mass flux has a significant effect on the heat release at the combustion zone in the chamber, which influences the coupling between the combustion heat release rate and the acoustic characteristics. As a result, the combustion stability is affected. It is the basic exciting mechanism of the combustion instability due to the propellant mass flow flux perturbation.

In the present work, the inlet mass flux perturbation coefficient and frequency were investigated. Based on the control effects of baffles on different combustion vibrations due to different perturbation coefficients and frequencies, the control capability of one baffle on the combustion instability was assessed. It is useful for the further optimized design of the rocket engine.

Figure 8 shows the transient pressure oscillation characteristics at the same check point when the same perturbation is added to one of the outermost circle injectors in the three kinds of chambers, respectively. Here, the mass flux perturbation coefficient and frequency are 2.0 and 5800 Hz, respectively. All of the results almost return to their natural frequencies of oscillations, shown in Fig. 8b. Especially, because of the particularity of the tangential-mode perturbation, two multiple frequencies including 10,937 and 16,406 Hz are also obviously presented. The maximum peak-to-peak dynamic pressures recorded at the check point are different, as shown in Fig. 8a. The maximum pressure peak-to-peak amplitude is up to 13.0% in the chamber without a baffle, whereas it is only about 8.0 and 2.0% in the chamber with a hub-and-three-blade baffle (baffle 1) and the chamber with a hub-and-six-blade baffle (baffle 2), respectively. This suggests that the control effects of a baffle on the combustion instability, which results from the mass flux perturbation at one of the outside circle injector inlets, are relatively obvious. Specifically, the control effect is better for the chamber with a hub-and-six-blade baffle. This conclusion can also be obtained by comparing the frequency amplitudes from Fig. 8b. The outside injector perturbation can easily result in tangential-mode resonance. Apparently, for the tangential-mode resonance, the more blades the baffle configuration has, the better the control effect is. Therefore, the six-blade baffle has a much better control effect than the three-blade baffle.

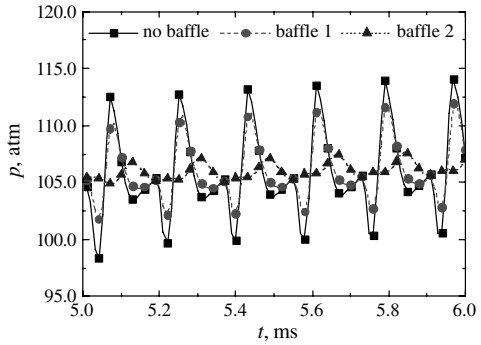

a) Pressure oscillations

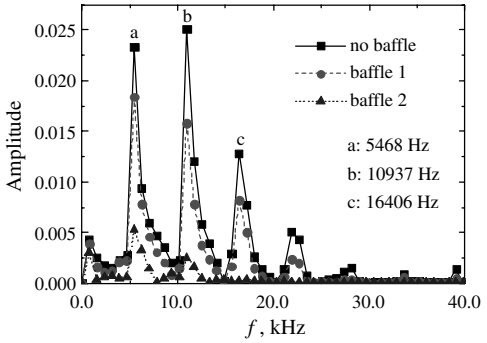

b) Frequency characteristics of the oscillations

Fig. 8 Pressure oscillation characteristics at $K = 2.0$, $f = 5800$ Hz at one of the outermost circle injectors.

E. Control Effects on Radial-Mode Instability

To understand the effect of baffles on the radial vibration, the transient combustion flowfields in the three chambers were simulated when adding perturbation with the same coefficient ($K = 2.0$) and

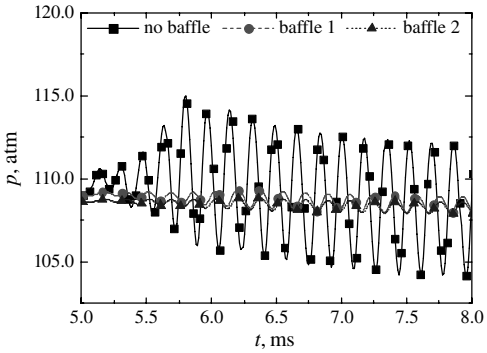

a) Pressure oscillations

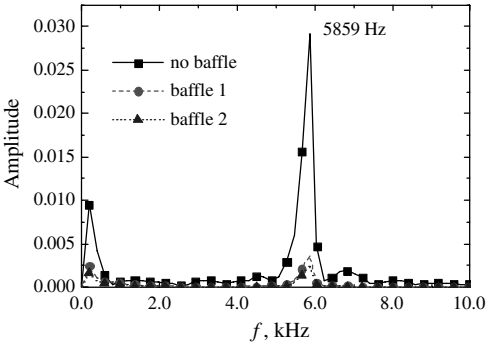

b) Frequency characteristics of the oscillations

Fig. 9 Pressure oscillation characteristics at $K = 2.0$, $f = 5800$ Hz at all of inside three circle injectors.

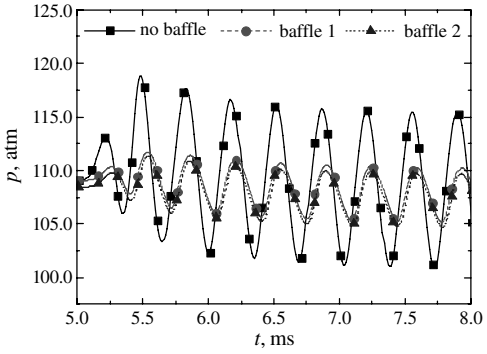

a) Pressure oscillations

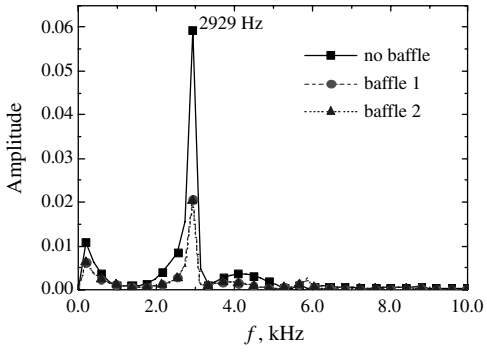

b) Frequency characteristics of the oscillations

Fig. 10 Pressure oscillation characteristics at $K = 2.0, f = 2900$ Hz at all of inside three circle injectors.

different frequencies ($f = 5800, 2900$ Hz) to all the inner three circle injectors. It is useful to further compare this with the control effect on the tangential vibration. The pressure oscillation characteristics at $K = 2.0$, $f = 5800$ Hz and $K = 2.0$, $f = 2900$ Hz are shown in Figs. 9 and 10, respectively. The control effect of the baffle on the pressure oscillation at $f = 5800$ Hz appears much better than that at $f = 2900$ Hz. The maximum pressure peak-to-peak amplitude is up to 8.0% in the chamber without a baffle, whereas it is only about 0.8 and 0.6% in the chamber with a hub-and-three-blade baffle and in the chamber with a hub-and-six-blade baffle, respectively. However, it is only reduced from 13.5 to 4.6% for the 2900 Hz perturbation. Although the injector perturbation in a baffle hub can easily result in radial-mode resonance, the control effects of two baffle configurations are similar for the radial-mode resonance. In addition, the effect is much better for the 5800 Hz perturbation. From the fast Fourier transform results for different baffles' configurations, the conclusion can also be obtained. The control extents can be evaluated by computing the depressing of frequency amplitudes, shown in Figs. 9b and 10b. It is 93.3 and 65.9% at 5800 and 2900 Hz, respectively.

F. Analysis of Control Mechanism

For the perturbation with the frequency of $f = 2900$ Hz added to all the inner three circle injectors, Figs. 11a and 11b show the pressure contour characteristics in a radial section and an axisymmetric section of the chamber without a baffle and the chamber with a hub-and-six-blade baffle at typical time points in an oscillation period, respectively. The radial-mode oscillation took place when the perturbation was added to all the inner three circle injectors. However, the radial-mode pressure oscillation was suppressed in the chamber with a hub-and-six-blade baffle, as is expected and shown in Fig. 11b. Additionally, the pressure contour characteristics in the axisymmetric section indicated that the longitudinal-mode oscillation took place in the chamber. Hence, the control mechanism is probably that the baffle changes the radial-mode acoustic waves to

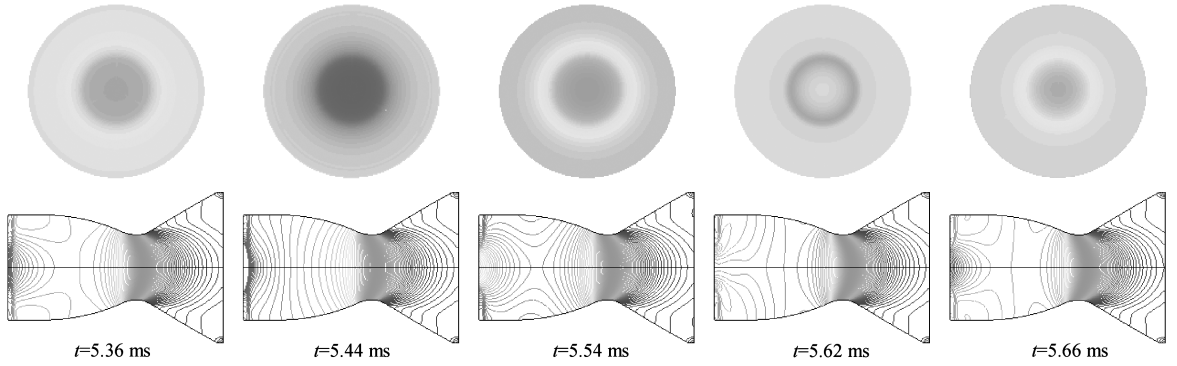

a) No baffle

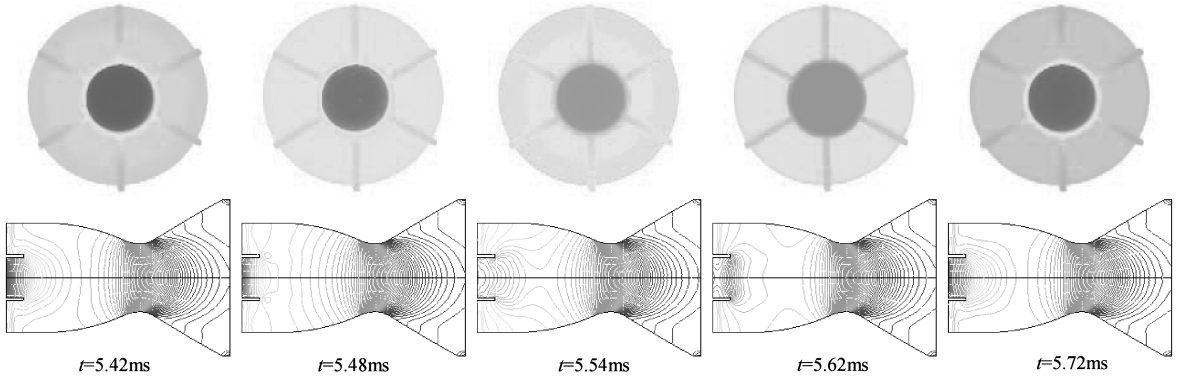

b) A hub-and-six-blade baffle

Fig. 11 Pressure contour characteristics at a radial section and an axisymmetric section of the two chambers at typical time points in an oscillation period.

longitudinal-mode waves within the baffle compartments. This is in agreement with the conclusion given in [8].

VI. Conclusions

The main oscillation frequency characteristic in the hot-firing tests of the YF-960 LOX/GH_2 rocket engine was reproduced and confirmed. The control effects of two kinds of baffles on combustion instability were studied by adopting the mass flow flux perturbing model developed in the work. The major conclusions are summarized as follows:

1) The simulated main frequencies were presented at about 1367, 2343, 3320, 5859, and 8203 Hz. These were in reasonable agreement with the oscillation phenomenon that appeared in the YF-960 hot tests.

2) By perturbing the steady-state mass flow flux field at one or some injector inlets for several cycles, the mass flow flux perturbing model could be used in analyzing combustion instability.

3) The control effect of the hub-and-six-blade baffle on the frequency of 5800 Hz tangential-mode resonance was much better than that of the hub-and-three-blade baffle. For the radial-mode resonance, the two kinds of baffles had similar control effects. However, the control effect was much better for the 5800 Hz oscillation compared with the 2900 Hz oscillation.

4) One of the baffle control mechanisms is probably that the baffle changes the radial-mode acoustic waves to longitudinal-mode waves within the baffle compartments.

This work has provided direct data for engineers to optimize the engine design. The data have been validated by the hot tests of the improved rocket engine. It is useful for further understanding the baffle eliminating mechanisms.

Acknowledgments

Financial support from the National Natural Science Foundation of China (50576105) is acknowledged. The support from the Beijing 11 Research Institute is gratefully acknowledged.

References

[1] Ned, P. H., and Herbert, E. S., "The Effect of Several Injector Face Baffle Configurations on Screech in a 20,000-Pound Thrust Hydrogen–Oxygen Rocket," NASA TM X-52251, Oct. 1966.

[2] Hersch, M., and Rice, E. J., "Gaseous-Hydrogen-Liquid-Oxygen Rocket Combustion at Supercritical Chamber Pressures," NASA TN D-4172, Sept. 1967.

[3] Morgan, C. J., and Sokolowski, D. E., "Longitudinal Instability Limits with a Variable Length Hydrogen–Oxygen Combustor," NASA TN D-6328, April 1972.

[4] Hutt, J. J., and Hulka, J. R., "Instability Phenomena in Liquid Oxygen/Hydrogen Propellant Rocket Engines," *Liquid Rocket Engine Combustion Instability*, edited by V. Yang, and W. E. Anderson, AIAA, Washington, D. C., 1995, Chap. 2.

[5] Wicker, J. M., Yoon, M. W., and Yang, V., "Linear and Non-Linear Pressure Oscillations in Baffled Combustion Chambers," *Journal of Sound and Vibration*, Vol. 184, No. 1, 1995, pp. 141–171. doi:10.1006/jsvi.1995.0309

[6] You, D., and Yang, V., "Linear Stability Analysis of Baffled Combustion Chamber with Radial and Circumferential Blades," AIAA Paper 2005-930, Jan. 2005.

[7] Kim, H. J., Lee, K. J., Seo, S., Han, Y. M., Seol, W. S., Lee, S. Y., and Ko, Y. S., "Stability Rating Tests of KSR-III Baffled Chamber Using Pulse Gun," AIAA Paper 2004-3364, July 2004.

[8] Sohn, C. H., Park, I. S., Kim, S. K., and Kim, H. J., "Acoustic Tuning of Gas–Liquid Scheme Injectors for Acoustic Damping in a Combustion Chamber of a Liquid Rocket Engine," *Journal of Sound and Vibration*, Vol. 304, Nos. 3–5, 2007, pp. 793–810. doi:10.1016/j.jsv.2007.03.036

[9] Kim, Y. M., Chen, C. P., and Ziebarth, J. P., "Numerical Simulation of Combustion Instability in Liquid-Fueled Engines," AIAA Paper 92-0775, Jan. 1992.

[10] Kim, Y. M., Chen, C. P., Ziebarth, J. P., and Chen, Y. S., "Prediction of High Frequency Combustion Instability in Liquid Propellant Rocket Engines," AIAA Paper 92-3763, July 1992.

[11] Frendi, A., Nesman, T., and Canabal, F., "Control of Combustion-Instabilities Through Various Passive Devices," AIAA Paper 2005-2832, May 2005.

[12] Mayer, W., Schik, A., Schaffler, M., and Tamura, H., "Injection and Mixing Processes in High Pressure Liquid Oxygen/Gaseous Hydrogen Rocket Combustors," *Journal of Propulsion and Power*, Vol. 16, No. 5, 2000, pp. 823–828. doi:10.2514/2.5647

[13] Haidn, O. J., and Habiballah, M., "Research on High Pressure Cryogenic Combustion," *Aerospace Science and Technology*, Vol. 7, No. 6, 2003, pp. 473–491. doi:10.1016/S1270-9638(03)00052-X

[14] Yang, V., "High-Pressure Combustion Chamber Dynamics," *International Symposium on Energy Conversion Fundamentals*, June 2004, pp. 1–52.

[15] Micci, M. M., and Gandilhon, D., "Shear Coaxial Injector LOX Droplet Measurements as a Function of Hydrogen Injection Temperature," *Atomization and Sprays*, Vol. 18, No. 1, 2008, pp. 85–96. doi:10.1615/AtomizSpr.v18.i1.30

[16] Zhuang, F. C., Nie, W. S., Zhao, W. T., and Liu, W. D., "Liquid Rocket Combustion Instability Analysis Methodology—Methods and Representative Examples," AIAA Paper 98-3690, July 1998.

[17] Zhuang, F. C., and Sun, J. G., "Effects of Swirl Coaxial Injector Parameters on LOX/GH_2 Engine Combustion Performance," AIAA Paper 2002-3697, July 2002.

[18] Feng, S. J., Cheng, Y. F., and Nie, W. S., "Combustion Instability Analysis in a Hydrogen–Oxygen Rocket Engine," AIAA Paper 2009-4864, Aug. 2009.

[19] Zhuang, F. C., *Theory, Model and Applications of Spray Combustion in LRE*, Vol. 1, National University of Defense Technology Press, Changsha, Hunan, People's Republic of China, 1995, pp. 61–64, 128–182, 220–271.

[20] Wang, Z. G., Liu, W. D., and Zhou, J., "Three-Dimension Numerical Simulation of Combustion Processes in LH_2/LOX Rocket Engines," AIAA Paper 99-2820, June 1999.

[21] He, B., Feng, S. J., Nie, W. S., and Zhang, J., "Research of the Gas–Liquid Equipment of LOX/GH_2 and Its Physical Parameters Under High Pressure Conditions," *Annual Conference of Academy of Chinese Engineering Thermophysics*, Academy of Chinese Engineering Thermophysics, Beijing, 2008.

[22] Wang, T. S., and Chen, Y. S., "Unified Navier–Stokes Flowfield and Performance Analysis of Liquid Rocket Engines," *Journal of Propulsion and Power*, Vol. 9, No. 5, 1993, pp. 678–685. doi:10.2514/3.23675

[23] Tabakoff, W., and Hamed, A., "Aerodynamic Effects on Erosion in Turbomachinery," *Tokyo Joint Gas Turbine Congress*, Tokyo, May 1977, pp. 574–580; alsoJapan Society Mechanical Engineering and American Society of Mechanical Engineers Paper 70.

[24] Reitz, R. D., "Modeling Atomization Processes in High-Pressure Vaporizing Sprays," *Atomisation and spray technology*, Vol. 3, 1987, pp. 309–337.

[25] O'Rourke, P. J., "Collective Droplets on Vaporizing Liquid Sprays," Ph.D. Dissertation, Princeton University, Princeton, NJ, 1981.

[26] Feng, S. J., Xie, Q. F., Nie, W. S., Duan, L. W., and Zhuang, F. C., "Active Control Simulation of Rocket Combustion Instability," AIAA Paper 2008-4582, July 2008.

[27] Zhou, L. X., *Dynamics of Multiphase Turbulent Reacting Fluid Flows*, Defense Industry Press, Beijing, Vol. 1, 2002, pp. 225–232.

[28] Zhou, J., Wang, Z. G., Zhao, W. T., and Zhuang, F. C., "Evaporation and Combustion of Nondilute Spray Droplet Group Under High Pressure," AIAA Paper 95-2428, July 1995.

T. Lin
Associate Editor